Supplementary Material

Structural and functional characterizations of HP0377, a thioredoxin-fold protein from *Helicobacter pylori*

Ji Young Yoon,[a] Jieun Kim,[b] Doo Ri An,[b] Sang Jae Lee,[c] Hyoun Sook Kim,[a,c] Ha Na Im,[b] Hye-Jin Yoon,[a] Jin Young Kim,[d] Soon-Jong Kim,[e] Byung Woo Han,[c*] and Se Won Suh[a,b*]

[a]Department of Chemistry, College of Natural Sciences, Seoul National University, Seoul 151-742, Republic of Korea, [b]Department of Biophysics and Chemical Biology, College of Natural Sciences, Seoul National University, Seoul 151-742, Republic of Korea, [c]College of Pharmacy, Seoul National University, Seoul 151-742, Republic of Korea, [d]Division of Mass Spectrometry, Korea Basic Science Institute, Ochang-eup Yeongudangiro 162, Cheongwon-gun, Chungbuk 363-883, Republic of Korea, and [e]Department of Chemistry, Mokpo National University, Chonnam, Republic of Korea

*Correspondence e-mail: bwhan@snu.ac.kr and sewonsuh@snu.ac.kr

Supplementary Information Content:

1. Supplementary materials and methods

1.1. Reductase assay with HP0518

The reductase assay using HP0518 was performed as described previously (Yoon *et al*., 2011). Briefly, the catalytic residue (Cys176) of HP0518 was modified using 5,5'-dithiobis(2-nitrobenzoic acid) (DTNB; Ellman's reagent) (Sigma). 2-Nitro-5-thiobenzoate (NTB^{2-}) produced from HP0518-NTB upon reduction by HP0377 or *H. pylori* DsbG (HP0231) was monitored by an increase in the absorbance at 412 nm. The absorbance was measured at an interval of 2 sec and the experiments were carried out in triplicate.

1.2. Insulin reduction assay

The ability of HP0377 and its R86A variant to catalyze insulin reduction in the presence of dithiothreitol (DTT) was determined as previously described (Holmgren, 1979). The reaction mixtures were prepared in cuvettes containing 131 μ*M* insulin, 0.1 *M* potassium phosphate buffer at pH 7.0, and 2 m*M* EDTA with 5 μ*M* enzyme in a final volume of 0.6 ml. The reactions were started by adding DTT to a final concentration of 0.33 m*M*. After thorough mixing, the optical density at 650 nm was measured for 120 min. As a negative control, the non-catalyzed reduction of insulin by DTT was monitored. *Escherichia coli* thioredoxin was used as a positive control.

1.3. Determination of the redox potentials

We determined the redox potentials of HP0377 and its R86A variant from the redox equilibrium with glutathione (Lafaye *et al*., 2009; Huber-Wunderlich & Glockshuber, 1998). Briefly, the protein at 1.0 μ*M* concentration was incubated under nitrogen atmosphere at 298 K in 100 m*M* sodium phosphate at pH 7.0, 1 m*M* EDTA containing 0.1 m*M* oxidized glutathione (GSSG) and increasing concentrations of reduced glutathione (GSH) for 16 h before recording the fluorescence emission on a JASCO FP-8300 spectrofluorometer. The relative amount of reduced HP0377 and its R86A variant at equilibrium (R) was measured using the fluorescence at 304 nm (excitation at 275 nm). HP0377 and its R86A variant show an increase in fluorescence intensity at 304 nm after full reduction of the oxidized form. Measurements were performed in triplicate, with three independent enzyme preparations. The equilibrium constant (K_{eq}) was determined by fitting the data to the following equation:

$$R = ([GSH]^2/[GSSG])/(K_{eq} + [GSH]^2/[GSSG]) \quad (1)$$

The redox potential (E_0') was calculated using the Nernst equation (Eqn. (2)) and a value of −240 mV as the standard redox potential of glutathione (Rost & Rapoport, 1964).

$$E_0' = -240 \text{ mV} - (RT/2F)\cdot \ln K_{eq} \quad (2)$$

1.4. Differential scanning calorimetry

Thermal stabilities of the HP0377 and its R86A variant proteins were assessed by measuring the melting temperature calorimetrically over the temperature range of 288–393 K at a scan rate of 90 K · h^{-1}. A VP-DSC calorimeter (MicroCal Inc.) was employed, using 150–200 m*M* protein in a 50 m*M* sodium phosphate buffer at pH 7.8. All measurements were performed in triplicate.

1.5. Determination of pK_a values

The cysteine pK_a was monitored by measuring the increased absorbance of UV light at 240 nm resulting from the formation of the thiolate anion (Noda *et al*., 1953). To determine the pK_a of the nucleophilic cysteine (Cys89) of HP0377, we recorded the specific absorbance of the thiolate anion at 240 nm (Nelson & Creighton, 1994). Measurements were carried out at 296 K in a buffer consisting of 10 m*M* potassium phosphate, 10 m*M* boric acid, 10 m*M* sodium succinate, 1 m*M* EDTA, and 200 m*M* KCl at pH 7.5. The initial assay volume was 2.0 ml and contained 30 µ*M* protein. The pH of the protein solution was lowered to 2.0 by stepwise addition of aliquots of 0.2 *M* HCl. The absorption of the sample at 240 and 280 nm was measured after correction for the absorption of the buffer alone. The extinction coefficient at 240 nm (ε_{240}) was calculated using the ratio of absorbance at 280 and 240 nm with the following equation (Eqn. 3):

$$\varepsilon_{240} = \varepsilon_{280} \frac{A_{240}}{A_{280}} \quad (3)$$

where A_{240}/A_{280} is the ratio of the absorbances of the protein at 240 nm and 280 nm, ε_{280} is the calculated extinction coefficient of HP0377 at 280 nm (19,370 M^{-1} cm^{-1}). Titrations were performed in triplicate and average values of ε_{240} were calculated. Data were plotted as a function of pH and the pK_a was determined by fitting a version of the Henderson-Hasselbalch equation to the data (Eqn. 4):

$$\varepsilon_{240}^{obs}\,(pH) = \varepsilon_{240}^{SH} + \frac{\varepsilon_{240}^{S-} - \varepsilon_{240}^{SH}}{1+10^{(pKa-pH)}} \quad (4)$$

where ε_{240}^{obs} (pH) is the observed extinction coefficient of the protein at 240 nm as a function of pH, ε_{240}^{SH} is the extinction coefficient of the protein at 240 nm when the cysteine residue is in the thiol form, and ε_{240}^{S-} is the extinction coefficient of the protein at 240 nm when the cysteine residue is in the thiolate form. Nonlinear regression was performed using Prism (GraphPad Software).

2. Supplementary results and discussion

2.1. Structural similarity search

We identified structurally similar proteins using the DALI server (Holm & Rosenström, 2010). Against the reduced HP0377 model, the highest Z-score was obtained with a domain of unknown function from *Methanosarcina mazei* Go1 (PDB code: 3IRA; an r.m.s. deviation of 2.4 Å for 127 equivalent C^{α} atom pairs, a Z-score of 12.3, and 15% sequence identity). The next highest Z-scores were obtained with the I75T variant of *E. coli* thioredoxin (Ren *et al*., 2009) (PDB code: 3DYR; an r.m.s. deviation of 1.9 Å for 105 equivalent C^{α} atom pairs, a Z-score of 11.9, and 19% sequence identity) and the *E. coli* cDsbD (Stirnimann *et al*., 2006) (PDB code: 2FWE; an r.m.s. deviation of 2.3 Å for 107 equivalent C^{α} atom pairs, a Z-score of 11.8, and 18% sequence identity).

The *M. mazei* Go1 domain of unknown function has additional α-helices at both N- and C-termini compared to the classic thioredoxin fold (Supplementary Fig. S2). The thioredoxin-like folds of *E. coli* thioredoxin I75T variant and cDsbD are essentially identical to each other and have an N-terminal extension (β1 and α1) only (Supplementary Fig. S2). A structural difference between them is the replacement of β5 of the *E. coli* thioredoxin I75T variant with a 3_{10} helix in cDsbD. HP0377 is unique with three distinct structural features, when it is compared to the classic thioredoxin fold. It has an extra 3_{10} helix (η1; Lys57–Tyr60) and a short β-strand (β0; Ser72–Ile73) at the N-terminus, and a 3_{10} helix (η2; Lys191–Gln193) and an α-helix (α4; Asp198–Ser216) at the C-terminus (Supplementary Fig. S2). In addition, it has an extra two-stranded antiparallel β-sheet (β3–β4; Glu125–Ser142) inserted between the β1-α1-β2 motif and the connecting helix α2 of the thioredoxin fold. This structural feature of HP0377 futher supports the previous suggestion that certain points in the thioredoxin fold can tolerate insertions without disruption of the overall structure (Martin, 1995).

In bovine glutathione peroxidase (PDB code: 1GP1; Epp *et al*., 1983) and *E. coli* DsbA (PDB code: 1DSB; Martin *et al*., 1993), 46 and 75 residues are inserted between β2 and α2 of the classic thioredoxin fold, respectively (Martin, 1995). The inserted residues of bovine glutathione peroxidase are folded into a meandering loop containing a short strand and a helix. The inserted residues of *E. coli* DsbA are folded into a helical domain. The internal insertion in glutathione peroxidase is located at the tetrameric interfaces. In *E. coli* DsbA, the interface

between the helical domain and the thioredoxin-fold domain provides a hydrophobic patch for binding a substrate peptide from SigA (Paxman *et al*., 2009). Unlike *E. coli* DsbA, the internally inserted region of HP0377 lies in a remote location from the active site and does not appear to provide a hydrophobic surface patch for binding its substrates. Unlike glutathione peroxidase, the internal insertion of HP0377 does not participate in the oligomer formation in our crystal structure. Our sedimentation equilibrium experiment also indicates that HP0377 exists as monomers in solution.

An extension at the C-terminus is present in glutathione S-transferase from human placenta (PDB code: 1GSS; Reinemer *et al*., 1992) and protein disulfide isomerase (PDI) from yeast (PDB code: 2B5E; Tian *et al*., 2006). In human glutathione S-transferase, a helical domain consisting of 127 residues is appended to the C-terminus of the classic thioredoxin fold and helps to stabilize the binding of glutathione and electrophilic substrates (Reinemer *et al*., 1992). In yeast PDI, the so-called a' thioredoxin domain is followed by a C-terminal extension consisting of an α-helical tail of 19 residues and disordered 18 residues, which are rich in negatively charged residues. The N-terminal part of the C-terminal α-helix makes hydrophobic interactions with the a' thioredoxin domain and plays an important role in stabilizing the a' thioredoxin domain (Tian *et al*., 2006). In HP0377, the C-terminal extension is composed of 27 residues (Lys191–Lys217) and it generates a predominantly positively charged surface on the side of the protein molecule where the active site faces the solvent. It may stabilize the thioredoxin-fold domain through the electrostatic and hydrophobic interactions (Supplementary Fig. S3) and may provide an extended surface for recognition of the binding partners.

2.2. HP0377 displays disulfide reductase activity

To demonstrate the disulifide reductase activity of HP0377, we used insulin reduction assay (Holmgren, 1979). The insulin reduction assay is a general method for measuring an oxidoreductase activity, specifically the reductase activity of a protein. It monitors precipitation of the insulin B-chain, which results from reduction of the interchain disulfides. Many thioredoxin-like oxidoreductases, including DsbA, DsbC, and thioredoxin from *E. coli*, are active in this assay. Both HP0377 and its R86A variant catalyzed the reduction of insulin in the presence of DTT. Their reaction lag times are 22 and 26 min, respectively, which are shorter than the negative control (30 min for DTT only) (Supplementary Table S1 and Fig. S10). The HP0377 R86A variant is slightly less active than HP0377, supporting the notion that Arg86 influences the redox property of HP0377.

2.3. Determination of redox potentials and pK_a values of the nucleophilic cysteine

The redox potentials of HP0377 and its R86A variant were determined to be −180 and −195 mV, respectively (Supplementary Table S1 and Fig. S11*a*). For comparison, reductases such as *E. coli* thioredoxin, *B. subtilis* ResA, *E. coli* DsbC, *E. coli* CcmG, *Bradyrhizobium japonicum* CcmG, and *B. japonicum* TlpA exhibit redox potentials of −270, −256, −140, −178, −217, and −256 mV, respectively (Mössner *et al*., 1998; Lewin *et al*., 2008; Rozhkova *et al*., 2004; Ouyang *et al*., 2006; Fabianek *et al*., 1997; Mohorko *et al*., 2012). In contrast, the redox potential of *E. coli* DsbA is −122 mV (Rozhkova *et al*., 2004). The measured redox potential of HP0377 is close to those of *E. coli* DsbC, *E. coli* CcmG, and *B. japonicum* CcmG, indicating that HP0377 could similarly function as a reductase. We also determined the melting temparatures of oxidized and reduced HP0377 (Supplementary Table S1). The data shows that the oxidized form of HP0377 is slightly more stable than the reduced form, consistent with the suggested role of HP0377 as a reductase. Similarly, the oxidized form of reducing proteins like *E. coli* thioredoxin and *Neisseria gonorrhoeae* TlpA exhibited greater thermal stability than the reduced form (Ladbury *et al*., 1994; Achard *et al*., 2009).

To further characterize HP0377 as an oxidoreductase, we measured the pK_a value of Cys89, the solvent-exposed nucleophilic cysteine in the active site, by monitoring the pH dependent changes in ε_{240}. The pH dependence of ε_{240} for HP0377 and its R86A variant showed a total change of 4,200 M^{-1} cm^{-1} and 3,500 M^{-1} cm^{-1}, respectively (Supplementary Fig. S11*b*). This result agrees with the reported change in ε_{240} of 4,000 M^{-1} cm^{-1} for a single thiolate (Noda *et al*., 1953). The pK_a value of HP0377 Cys89 is measured to be 3.2 (Supplementary Table S1), which is much lower than the typical value of ~8.5 for cysteine residues (Nelson & Creighton, 1994). The measured pK_a value of HP0377 is comparable to those of the solvent-exposed nucleophilic cysteine in *E. coli* DsbC and DsbA (4.1 and 3.3, respectivley) (Sun & Wang, 2000; Huber-Wunderlich & Glockshuber, 1998). The lowered pK_a of the reactive cysteine determines reactivity in thiol-disulfide exchange reactions (Heras *et al.*, 2008). CcmG (DsbE) proteins in Gram-negative bacteria have been shown to be weak reductants, whose solvent-exposed active site cysteines have pK_a values around 6.5–6.8 (Goulding *et al*., 2004). Compared to other CcmG proteins involved in cytochrome *c* maturation, the unusually low pK_a value of Cys89 in HP0377 may be associated with its recognition of a broad range of substrates.

It was observed that a correlation exists between the pK_a value of the nucleophilic cysteine and standard redox potential of several thioredoxin-fold proteins (Roos *et al.*, 2013;

Huber-Wunderlich & Glockshuber, 1998; Mössner *et al*., 1998). The measured pK_a value and the redox potential of HP0377 deviate a little from the observed correlation. However, a much larger deviation from the relationship was reported for *E. coli* DsbD γ-domain (Roos *et al.*, 2013).

The pK_a value of Cys89 in HP0377 R86A variant is 3.3 (Supplementary Table S1). It appears that the influence of Arg86 on the ionization behavior of Cys89 is limited and other factors play a dominant role. In *E. coli* DsbA, elimination of all charged residues in the neighborhood of the active site had a negligible impact on the pK_a of its nucleophilic cysteine (Jacobi *et al.*, 1997). It was also reported that the stabilization of the thiolate by hydrogen bonds with neutral groups, for example, with backbone amides plays a major role (Foloppe & Nilsson, 2007; Mieyal *et al*., 1991; Roos *et al.*, 2013). In the reduced HP0377, the thiolate of Cys89 is stabilized by making hydrogen bonds with the backbone amide and the side chain of Cys92 and the hydroxyl group of Thr155, and by interacting electrostatically with the positive end of helix α1a dipole and Arg86.

Supplemental references

Achard, M. E., Hamilton, A. J., Dankowski, T., Heras, B., Schembri, M. S., Edwards, J. L., Jennings, M. P. & McEwan, A. G. (2009). *Infect Immun.* **77**, 4934–4939.

Epp, O., Ladenstein, R. & Wendel, A. (1983). *Eur. J. Biochem.* **133**, 51–69.

Fabianek, R. A., Huber-Wunderlich, M., Glockshuber, R., Künzler, P., Hennecke, H. & Thöny-Meyer, L. (1997). *J. Biol. Chem.* **272**, 4467–4473.

Foloppe, N. & Nilsson, L. (2007). *J. Mol. Biol.* **372**, 798–816.

Goulding, C. W., Apostol, M. I., Gleiter, S., Parseghian, A., Bardwell, J., Gennaro, M. & Eisenberg, D. (2004). *J. Biol. Chem.* **279**, 3516–3524.

Heras, B., Kurz, M., Jarrott, R., Shouldice, S. R., Frei, P., Robin, G., Cemazar, M., Thöny-Meyer, L., Glockshuber, R. & Martin, J. L. (2008). *J. Biol. Chem.* **283**, 4261–4271.

Holm, L. & Rosenström, P. (2010). *Nucleic Acids Res.* **38**, W545–W549.

Holmgren, A. (1979). *J. Biol. Chem.* **254**, 3664–3671.

Huber-Wunderlich, M. & Glockshuber, R. (1998). *Fold. Des.* **3**, 161–171.

Jacobi, A., Huber-Wunderlich, M., Hennecke, J. & Glockshuber, R. (1997). *J. Biol. Chem.* **272**, 21692–21699.

Ladbury, J. E., Kishore, N., Hellinga, H. W., Wynn, R. & Sturtevant, J. M. (1994). *Biochemistry,* **33**, 3688–3692.

Lafaye, C., Iwema, T., Carpentier, P., Jullian-Binard, C., Kroll, J. S., Collet, J. F. & Serre, L. (2009). *J. Mol. Biol.* **392**, 952–966.

Lewin, A., Crow, A., Hodson, C. T., Hederstedt, L. & Le Brun, N. E. (2008). *Biochem. J.* **414**, 81–91.

Martin, J. L. (1995). *Structure*, **3**, 245–250.

Martin, J. L., Bardwell, J. C. & Kuriyan, J. (1993). *Nature*, **365**, 464–468.

Mieyal, J. J., Starke, D. W., Gravina, S. A. & Hocevar, B. A. (1991). *Biochemistry* **30**, 8883–8891.

Mohorko, E., Abicht, H. K., Bühler, D., Glockshuber, R., Hennecke, H. & Fischer, H. M. (2012). *FEBS Lett*. **586**, 4094–4099.

Mössner, E., Huber-Wunderlich, M. & Glockshuber, R. (1998). *Protein Sci*. **7**, 1233–1244.

Nelson, J. W. & Creighton, T. E. (1994) *Biochemistry*, **33**, 5974–5983.

Noda, L. H, Kuby, S. A. & Lardy, H. A. (1953). *J. Am. Chem. Soc.* **75**, 913–917.

Ouyang, N., Gao, Y. G., Hu, H. Y. & Xia, Z. X. (2006). *Proteins*, **65**, 1021–1031.

Paxman, J. J., Borg, N. A., Horne, J., Thompson, P. E., Chin, Y., Sharma, P., Simpson, J. S., Wielens, J., Piek, S., Kahler, C. M., Sakellaris, H., Pearce, M., Bottomley, S. P., Rossjohn, J. & Scanlon, M. J. (2009). *J. Biol. Chem.* **284**, 17835–17845.

Reinemer, P., Dirr, H. W., Ladenstein, R., Huber, R., Lo Bello, M., Federici, G. & Parker, M. W. (1992). *J. Mol. Biol.* **227**, 214–226.

Ren, G., Stephan, D., Xu, Z., Zheng, Y., Tang, D., Harrison, R. S., Kurz, M., Jarrott, R., Shouldice, S. R., Hiniker, A., Martin, J. L., Heras, B. & Bardwell, J. C. (2009). *J. Biol. Chem.* **284**, 10150–10159.

Roos, G., Foloppe, N. & Messens, J. (2013). *Antioxid. Redox Signal.* **18**, 94–127.

Rost, J. & Rapoport, S. (1964). *Nature*, **201**, 185.

Rozhkova, A., Stirnimann, C. U., Frei, P., Grauschopf, U., Brunisholz, R., Grütter, M. G., Capitani, G. & Glockshuber, R. (2004). *EMBO J.* **23**, 1709–1719.

Stirnimann, C. U., Rozhkova, A., Grauschopf, U., Böckmann, R. A., Glockshuber, R., Capitani, G. & Grütter, M. G. (2006). *J. Mol. Biol.* **358**, 829–845.

Sun, X. X. & Wang, C. C. (2000). *J. Biol. Chem.* **275**, 22743–22749.

Tian, G., Xiang, S., Noiva, R., Lennarz, W. J. & Schindelin, H. (2006). *Cell*, **124**, 61–73.

Yoon, J. Y., Kim, J., Lee, S. J., Kim, H. S., Im, H. N., Yoon, H. J., Kim, K. H., Kim, S. J., Han, B. W. & Suh, S. W. (2011). *FEBS Lett*. **585**, 3862–3867.

Supplementary Table S1. Redox properties of HP0377 (33–221) and its R86A variant

Protein	Insulin reduction assay [lag time (min)]	Redox potential (mV)	pK_a of nucleophilic Cys	Tm (K)	
				Reduced	Oxidized
HP0377 wt	22	– 180	3.2	332	338
HP0377 R86A	26	– 195	3.3	345	340
E. coli thioredoxin	6	– 270[a]	7.1[a]	346[b, c]	358[b, c]
DTT	30	–	–	–	–

[a] Mössner *et al*., 1998, [b] Ladbury *et al*., 1993, [c] Ladbury *et al*., 1994

Supplementary Fig S1. Proteins sharing similar modifications of the classic thioredoxin fold with HP0377. (*a*) Schematic representation of the secondary structure elements of HP0377, *B. subtilis* ResA, *E. coli* CcmG, *B. japonicum* CcmG, and *B. japonicum* TlpA. α-Helices, 3_{10}-helices, β-strands, and loops are shown as cylinders, flat cylinders, arrows, and solid lines, respectively. The characteristic secondary structure elements of the thioredoxin fold (β1-α1-β2 and β3-β4-α3 motifs linked by a short connecting α helix α2) are shown in gray. The dotted line indicates the disordered region. Modifications of the thioredoxin fold in HP0377, *B. subtilis* ResA, *E. coli* CcmG, *B. japonicum* CcmG, and *B. japonicum* TlpA are colored in green, red, violet, orange, and hotpink, respectively. (*b*) Ribbon diagram of the structures of HP0377, *B. subtilis* ResA (PDB code: 1ST9), *E. coli* CcmG (PDB code: 2B1K), *B. japonicum* CcmG (PDB code: 1KNG), and *B. japonicum* TlpA (PDB code: 1JFU). Thioredoxin domains are shown in gray and the modifications are shown in the same color scheme as in (*a*).

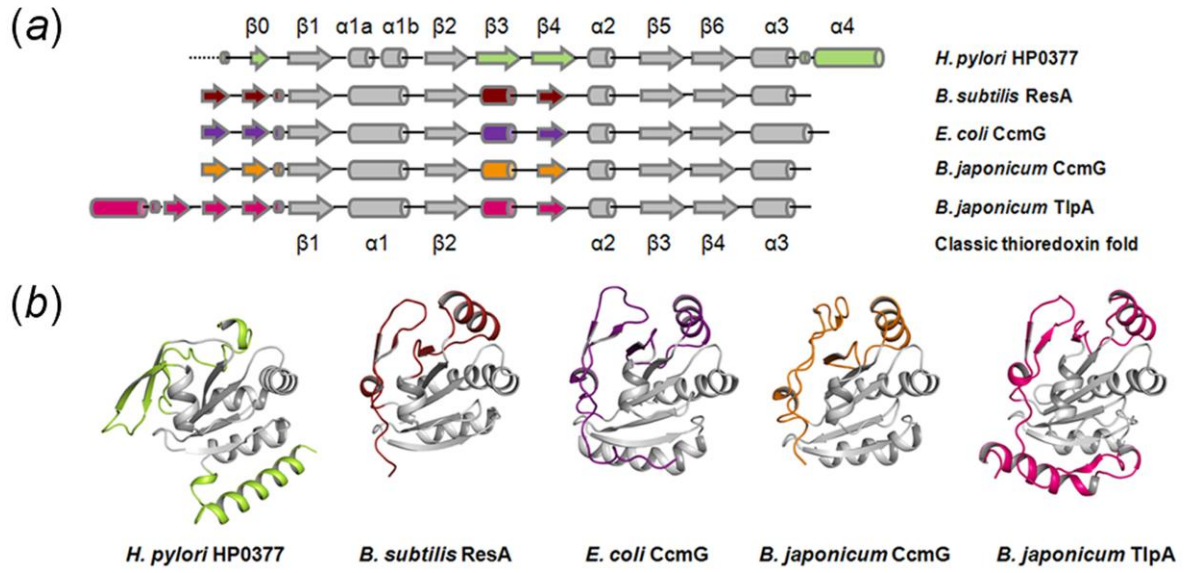

Supplementary Fig S2. Proteins showing structural similarities to HP0377 as indicated by a DALI search. (*a*) Schematic representation of the secondary structure elements of HP0377, *M. mazei* unknown function domain, *E. coli* thioredoxin I75T variant, and *E. coli* DsbD C-terminal domain. α-Helices, 3_{10}-helices, β-strands, and loops are shown as cylinders, flat cylinders, arrows, and solid lines, respectively. The characteristic secondary structure elements of the thioredoxin fold (β1-α1-β2 and β3-β4-α3 motifs linked by a short connecting α-helix α2) are shown in gray. Modifications of the thioredoxin fold in HP0377, *M. mazei* unknown function domain, *E. coli* thioredoxin I75T variant, and *E. coli* DsbD C-terminal domain are colored in green, teal, purple, and pink, respectively. The dashed lines indicate the absent secondary structures and the dotted line indicates the disordered region. (*b*) Ribbon diagram of the structures of HP0377, the unknown function domain from *M. mazei* (PDB code: 3IRA), thioredoxin I75T variant from *E. coli* (PDB code: 3DYR), and DsbD C-terminal domain from *E. coli* (PDB code: 2FWE). Thioredoxin domains are shown in gray and the modifications are shown in the same color scheme as in (*a*).

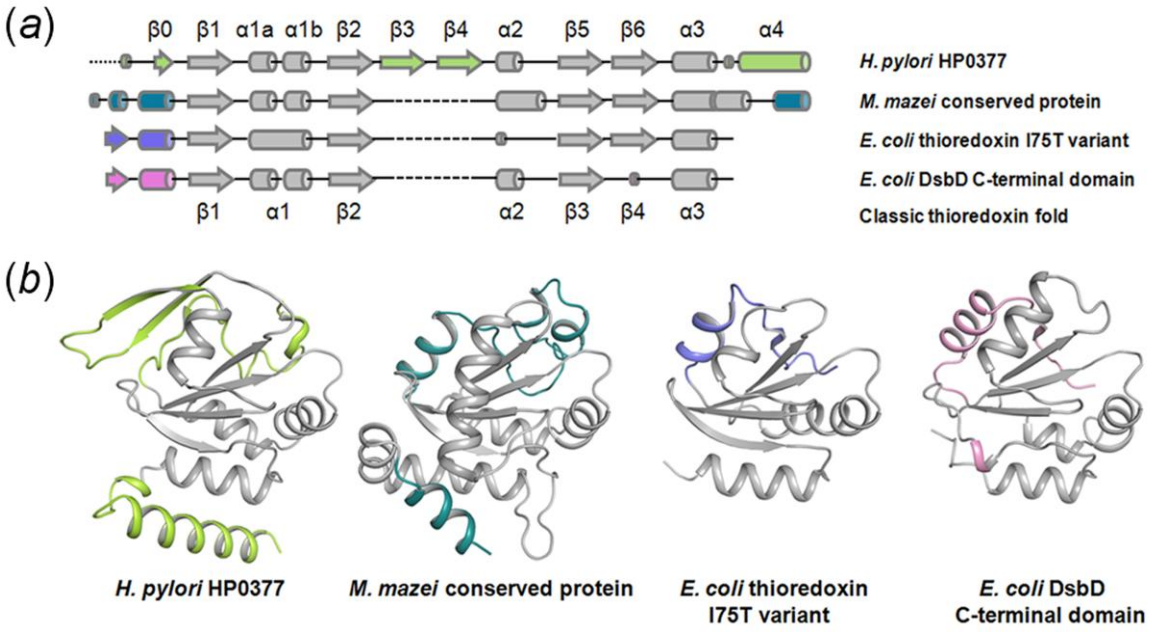

Supplementary Fig S3. Interactions of the C-terminal α-helix (α4) with neighboring secondary structure elements in HP0377. (*a*) Stereoview of hydrophobic interactions. (*b*) Stereoview of hydrogen bonds (dotted lines).

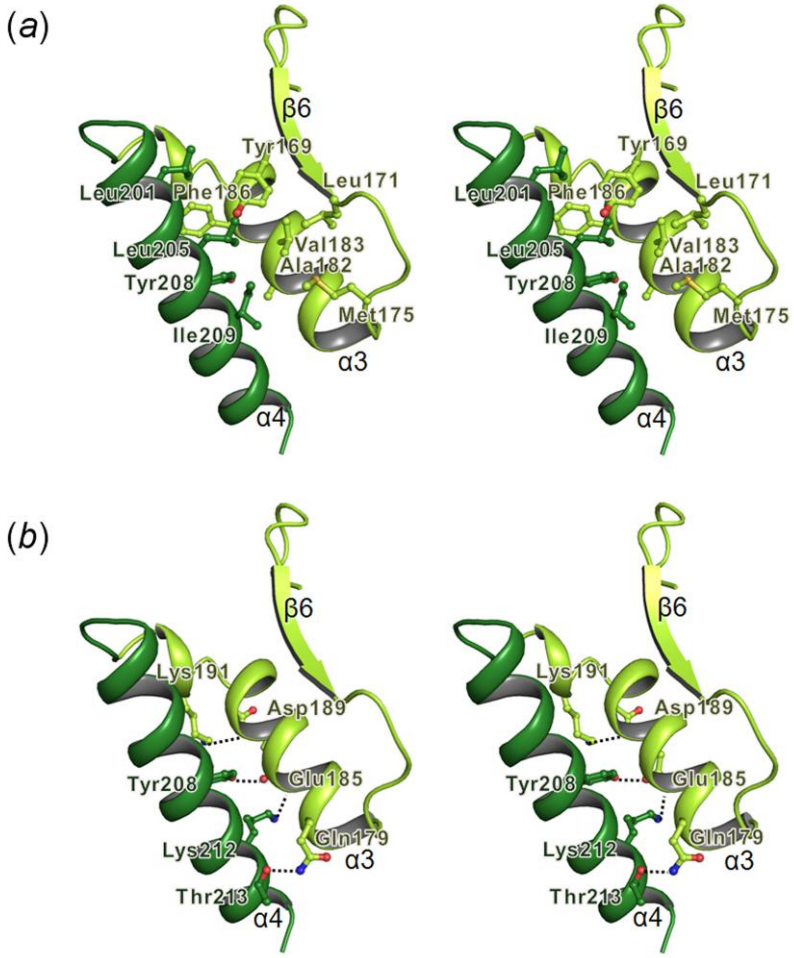

Supplementary Fig S4. A sedimentation equilibrium distribution of reduced HP0377 in the presence of TCEP. (*a*) The protein concentration of HP0377 (33–221) was 10.4 μ*M*. The circles are experimental absorbance data at 280 nm, and the solid and dotted lines are the curves for homogeneous monomer (1x) and dimer (2x) models, respectively. The weighted root-mean-square (r.m.s.) errors for the monomer (1x) and dimer (2x) fits were 6.63×10^{-3} and 2.53×10^{-2}, respectively. (Inset) Distributions of the residuals for monomer (1x, circle) and dimer (2x, solid line) models. (*b*) The protein concentration of HP0377 (24–221) was 10.3 μ*M*. The squares are experimental data at 280 nm and the solid line is a fitting line for an ideal monomer (1x) model. The dotted line is a fitting line for an ideal dimer (2x) model. The r.m.s. errors for the monomer (1x) and dimer (2x) fits were 9.27×10^{-3} and 4.67×10^{-2}, respectively. (Inset) Distributions of the residuals for monomer (1x, square) and dimer (2x, circle) models. The random distributions of residuals for the monomer (1x) model indicate that both constructs of HP0377 exist as homogeneous monomers in solution.

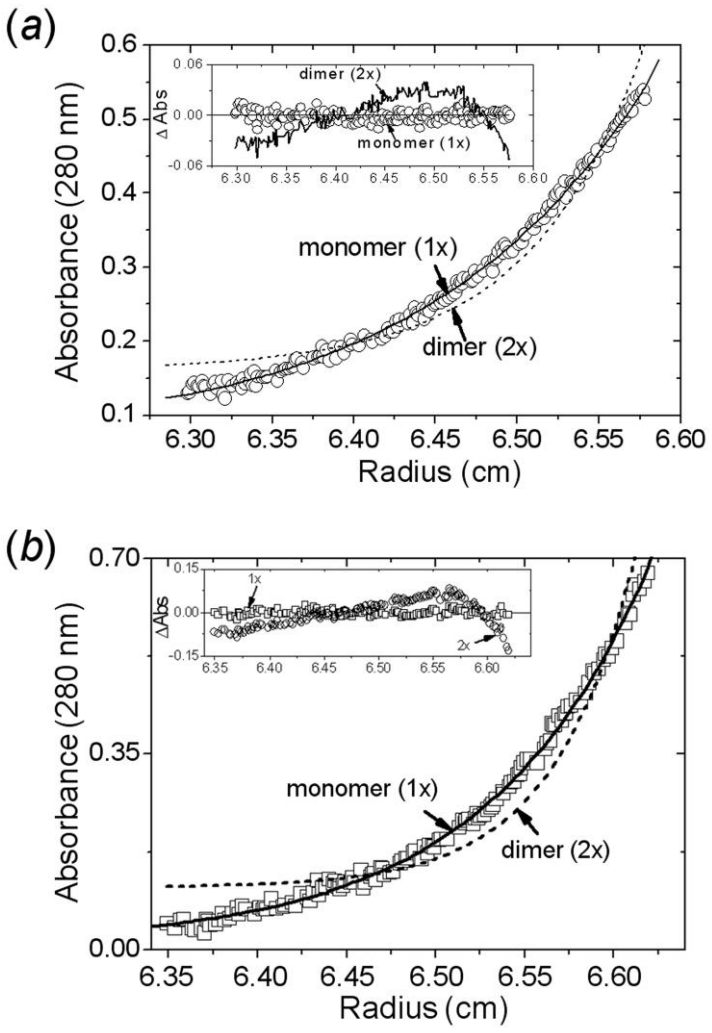

Supplementary Fig S5. Reductase assay of HP0377 and *H. pylori* DsbG (HP0231) using HP0518. Reduction of the HP0518-NTB adduct by reduced HP0377 or *H. pylori* DsbG (HP0231) was monitored by the absorbance at 412 nm.

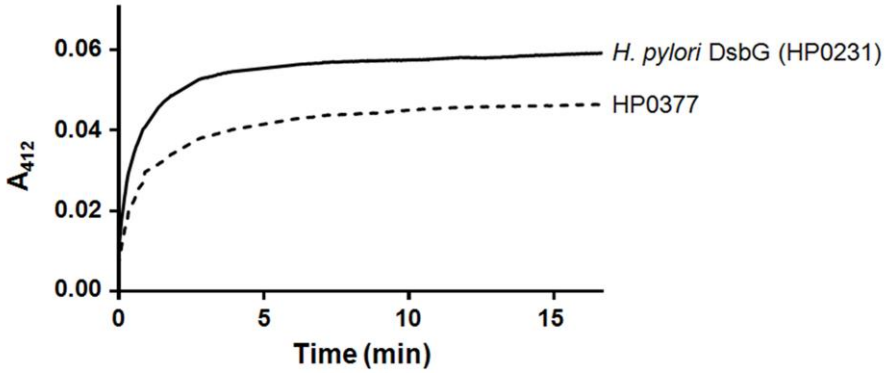

Supplementary Fig S6. Analysis of the complex formation between HP0377 C92A and HP0518. (*a*) The complex formed between HP0377 C92A and HP0518 was analyzed by size exclusion chromatography and multi-angle light scattering (SEC-MALS). Elution profiles for the reaction mixture between HP0377 C92A and HP0518-NTB (thin red solid lines) and HP0518 alone (thin blue solid line) are shown. The corresponding horizontal lines represent the measured mass obtained by SEC-MALS. (*b*) SDS-PAGE analysis of the HP0377 C92A–HP0518 complex formation. Lane M: prestained protein ladder. Lane 1: HP0377 C92A. Lane 2: HP0518. Lane 3: HP0377 C92A–HP0518 complex isolated by size exclusion chromatography, i.e., the high molecular mass peak in (*a*)].

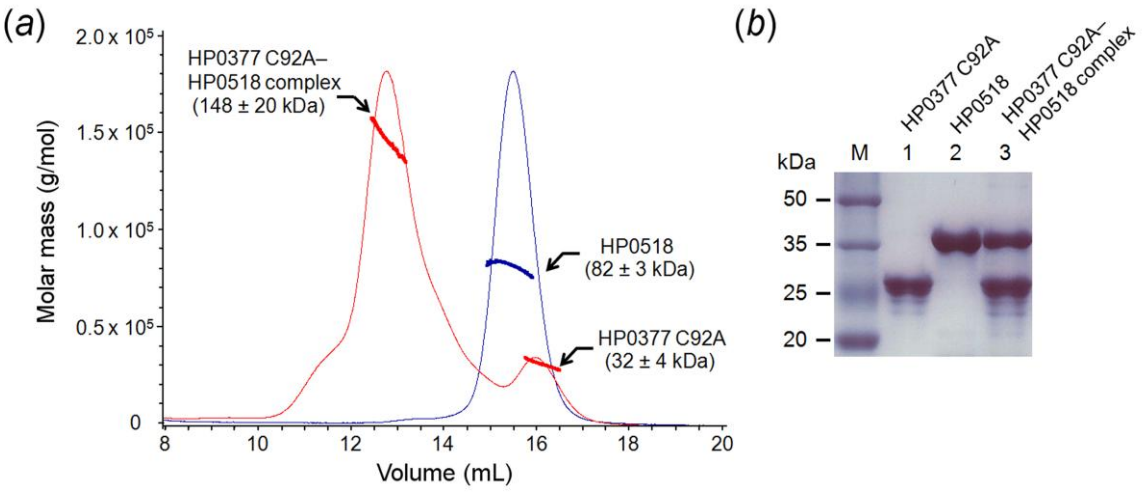

Supplementary Fig S7. SDS-PAGE analysis of the HP0377 C92A–HP0518 complex formation upon mixing with different amounts of HP0377 C92A. The molar stoichiometry of HP0377 C92A to HP0518 was 1:2 (lane 1) and 1:1 (lane 2). The complexes were separated by size exclusion chromatography and were subject to SDS-PAGE. The complex in lane 2 eluted slightly earlier than that in lane 1.

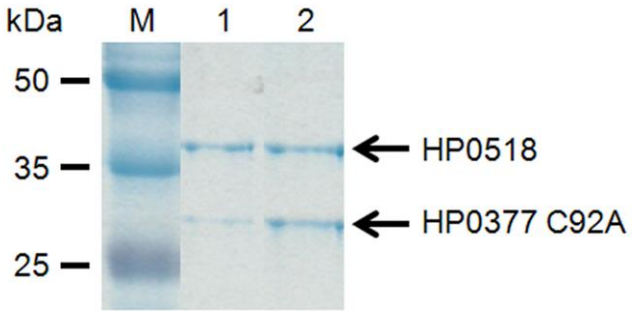

Supplementary Fig S8. MS/MS spectrum of the disulfide-bonded peptide ^{175}GCIAIENPLLSSYDK^{189}—^{87}NGCSYAER^{94} isolated from the HP0518–HP0377 C92A covalent complex by tryptic digestion. The fragments of HP0518 (residues 175–189; calculated mass = 1622.8 Da) and HP0377 C92A (residues 87–94; calculated mass = 898.9 Da) are marked by P1 and P2, respectively. The spectrum shows fragmentation characteristics of a disulfide linkage, including cysteine persulfides (P1 or P2 + 32 Da) and dehydroalanines (P1 or P2 – 34 Da).

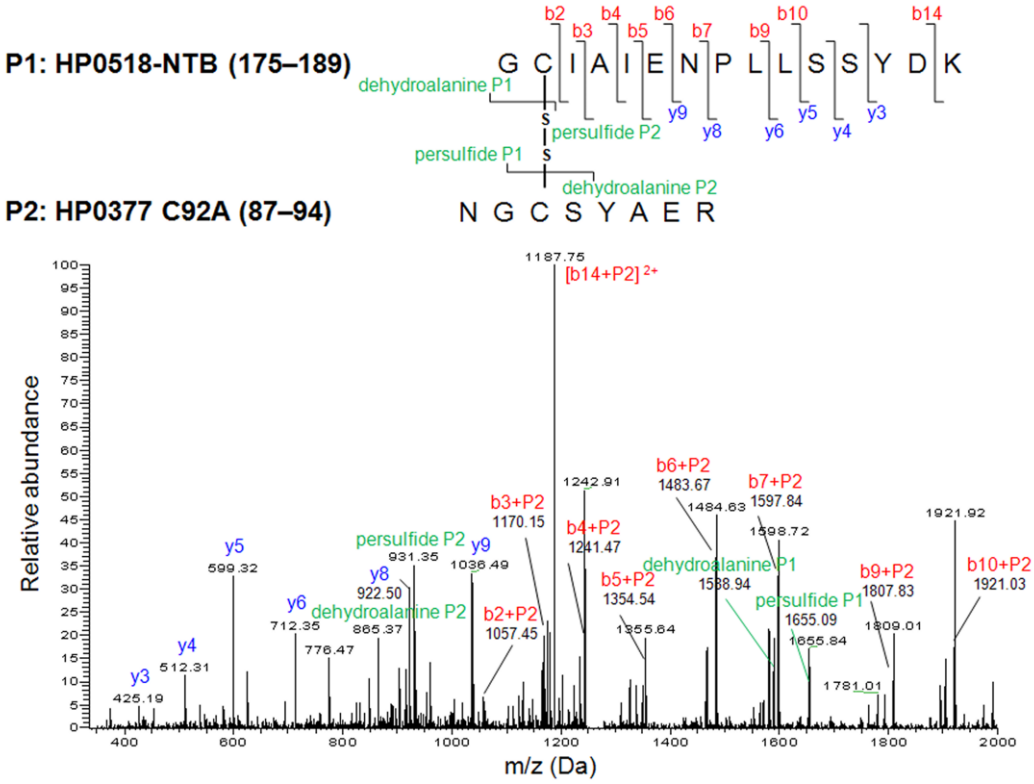

Supplementary Fig S9. Stereoview of the active site region after superimposing the CXXC motifs of reduced HP0377 (blue) and reduced *Bacillus subtilis* ResA (pale blue). Catalytic cysteine residues, the residue preceding the CXXC motif, and the residue preceding the *cis*-Pro residue are shown in ball and stick models with labelling. Secondary structure elements of both proteins are labeled.

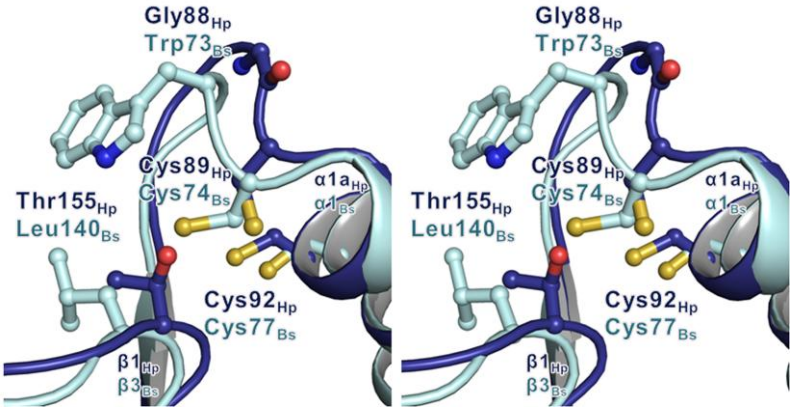

Supplementary Fig S10. Insulin reduction assay. The reactions were performed in the presence of DTT and a disulfide oxidoreductase (HP0377, HP0377 R86A variant, or *E. coli* thioredoxin) as well as in the presence of DTT only (as a negative control).

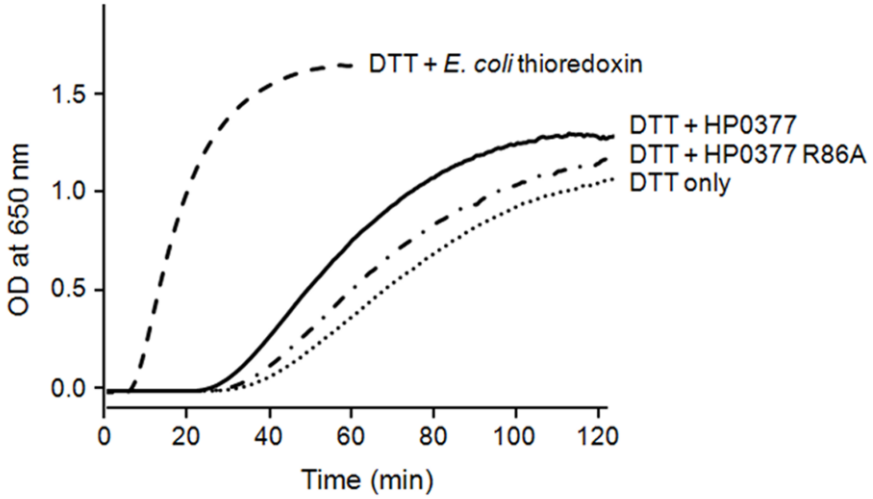

Supplementary Fig S11. Redox potential and pK_a of HP0377 (33–221) (●) and its R86A variant (□). (*a*) The fraction (R) of reduced HP0377 and its R86A variant at redox equilibrium with glutathione was estimated by measuring the tyrosine fluorescence of the protein at 304 nm (excitation at 275 nm) (*b*) Determination of the pK_a of the nucleophilic cysteine (Cys89). The absorbance at 240 nm of HP0377 and its R86A variant was measured at various pH values and ε_{240} values were fitted according to the Henderson-Hasselbach equation.

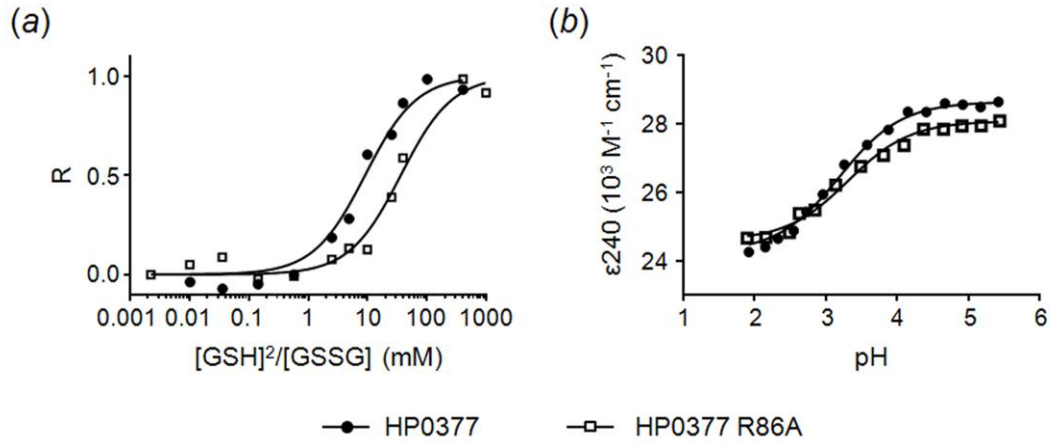

Supplementary Fig S12. Stereo view of the active site region after superimposing HP0377 with *E. coli* DsbC, *B. subtilis* ResA, and *Pseudomonas aeruginosa* CcmG. Catalytic cysteine residues and the residue preceding the *cis*-Pro are shown in ball and stick models. Secondary structure elements and residues of HP0377 are labeled.

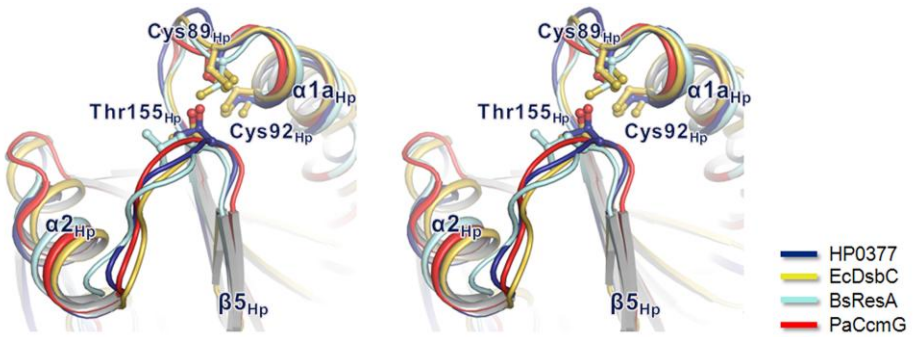

Supplementary Fig S13. Binding of PEG near the active site Cys89 of reduced HP0377. The electrostatic potential at the molecular surface is colored in blue and red according to positive and negative potentials, respectively. A bound PEG molecule is colored in orange surrounded by the $2mF_o - DF_c$ electron density (orange mesh) contoured at 1.0 σ level. The sulfur atom of Cys89 is denoted by S (left and right). Residues interacting with PEG are shown in the box as ball and stick (right) and are labeled.